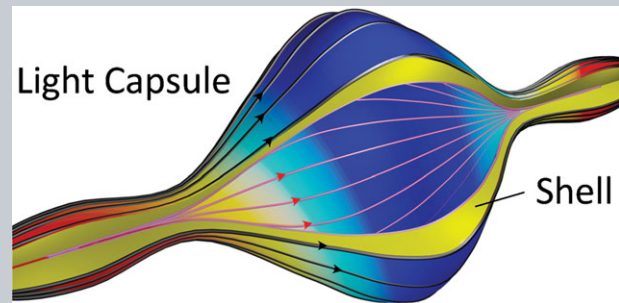**Abstract** Supersized darkness in three dimensions surrounded by all light in free space is demonstrated theoretically and experimentally in the visible regime. The object staying in the darkness is similar to staying in an empty light capsule because light just bypasses it by resorting to destructive interference. A binary-optical system is designed and fabricated based on achieving antiresolution (AR), by which electromagnetic energy flux avoids and bends smoothly around a nearly perfect darkness region. AR remains an unexplored topic hitherto, in contrast to the super-resolution for realizing high spatial resolution. This novel scheme replies on smearing out the point spread function and thus poses less stringent limitations upon the object's size and position since the created dark (zero-field) area reach 8 orders of magnitude larger than λ^2 in cross-sectional size. It functions very well with arbitrarily polarized beams in

three dimensions, which is also frequency scalable in the whole electromagnetic spectrum.

ORIGINAL PAPER

Three-dimensional visible-light capsule enclosing perfect supersized darkness via antiresolution

Chao Wan[1],[**], Kun Huang[1],[**], Tiancheng Han[1],[**], Eunice S. P. Leong[2], Weiqiang Ding[1], Lei Zhang[1], Tat-Soon Yeo[1], Xia Yu[3], Jinghua Teng[2], Dang Yuan Lei[4], Stefan A. Maier[5], Boris Luk'yanchuk[6], Shuang Zhang[7], and Cheng-Wei Qiu[1],[*]

1. Introduction

It is well known that the point spreading function (PSF) (Fig. 1a) dictates the performance of an optic focusing system [1, 2], so a sharp PSF with a strong main lobe and a weak sidelobe (Fig. 1b) is highly desired for realizing high spatial resolution [3]. In the past decade, much research effort has been dedicated to narrowing the PSF so as to achieve super-resolution and beat the diffraction limit [4–13]. Concurrently, significant effort in optical super-resolution has been devoted to the development of various optical microscopy techniques (e.g., stimulated emission depletion microscopy [12] and stochastic optical reconstruction microscopy [13]) based on molecular labeling, nonlinear optical saturation, luminescence, and excitation/de-excitation of fluorophores.

One interesting question beyond the current focus is what new interesting phenomena and applications exist if one pushes the limit toward the other extreme, i.e. sup-

pressing and flattening the main lobe in the PSF until it has completely vanished and elevating the sidelobe (Fig. 1d), which is completely inverse to the manipulation of super-resolution in Fig. 1b. For this inversely manipulated PSF, a point source at the object plane leads to a large-radius ring intensity, resulting in the dis-resolved imaging at the imaging plane. This new scheme, defined in our concept as antiresolution (AR), can be obtained by designing an imaging system made of concentric dielectric grooves together with a focusing lens. Antiresolution only denotes the inverse manipulation of the PSF in contrast with that of the PSF for super-resolution (refer to Figs. 1b and d). Antiresolution has a relocated PSF with the ring-shaped intensity. Antiresolution does not mean this optical system can not resolve the objects under other conditions, e.g. the objects can still be resolved if one resorts to the deconvolution technique. Such implementation creates a macroscopic spatial region with nearly perfect dark region where the energy flux of light approaches zero. The darkness in PSF spreads

---

[1] Department of Electrical and Computer Engineering, National University of Singapore, 4 Engineering Drive 3, Singapore 117576, Singapore
[2] Institute of Materials Research and Engineering, Agency for Science, Technology and Research, 3 Research Link, Singapore 117602, Singapore
[3] Singapore Institute of Manufacturing Technology, Agency for Science, Technology and Research, 71 Nanyang Drive, Singapore 638075, Singapore
[4] Department of Applied Physics, The Hong Kong Polytechnic University, Kowloon, Hong Kong
[5] The Blackett Laboratory, Department of Physics, Imperial College London, London SW7 2 AZ, UK
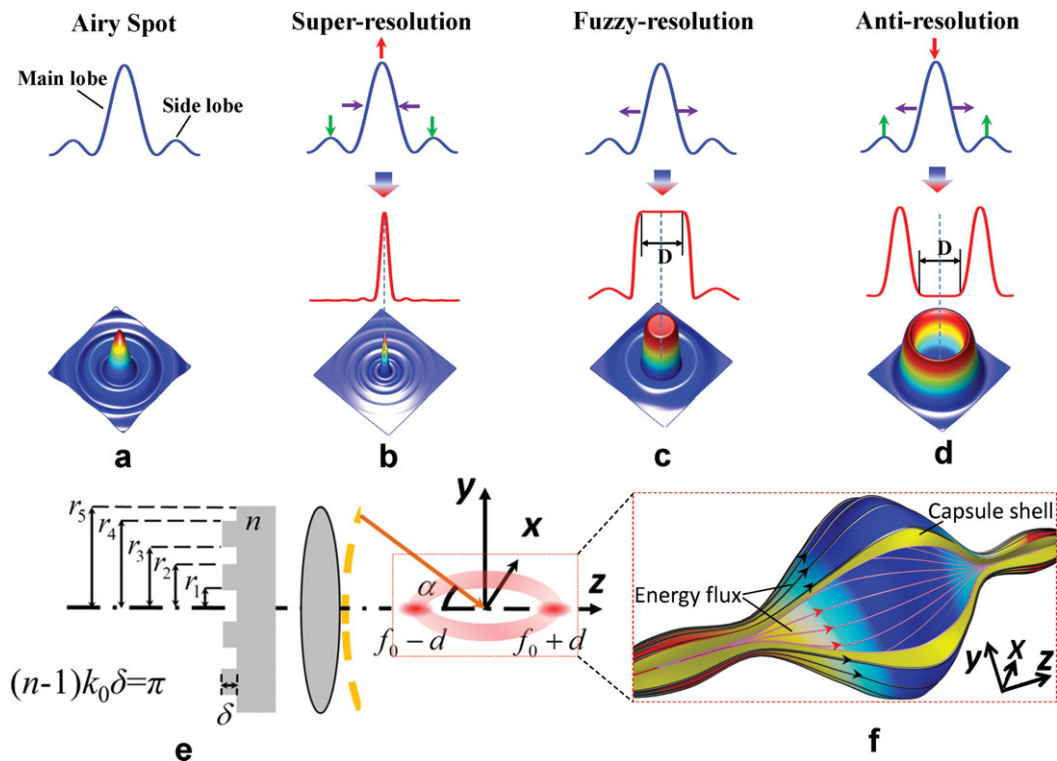[6] Data Storage Institute, Agency for Science, Technology and Research, 5 Engineering Drive 1, Singapore 117608, Singapore
[7] School of Physics & Astronomy, University of Birmingham, Birmingham B15 2TT, UK
[**]These authors contribute equally to this work.
[*]Corresponding author: e-mail: eleqc@nus.edu.sg

Figure 1 Evolution from super-resolution to antiresolution. The PSF of a traditional optical imaging system has the form of Airy spot (a). The super-resolution in (b) is achieved by narrowing the PSF, enhancing the mainlobe as well as suppressing the sidelobe. If we just widen the PSF without any disposing of mainlobe and sidelobe in PSF, the fuzzy-resolution (c) leading to degradation in imaging can be obtained. One completely inverse case of (b) in manipulation of PSF is widening the PSF, suppressing the mainlobe and enhancing the sidelobe so that the PSF in the region D ($\gg \lambda$) completely vanishes, which is the concept of antiresolution (d). (e) The scheme for realizing a visible-light capsule based on antiresolution with binary phase on. (f) The 3D optical capsule based on AR concept. Energy flows in the capsule whose outer and inner boundaries are shown by the black and red curves, respectively.

in the focal region for the uniform variation of energy flux in the homogenous medium, resulting in a huge darkness region surrounded by visible light, which looks like a three-dimensional "optical capsule". A three-dimensional object placed in the visible-light capsule does not cause scattering due to the supersized darkness and the scene behind the object can therefore be illuminated and observed through the light (capsule shell) surounding the darkness. The challenge is two-fold: (1) the dark region must have a remarkably large volume of smeared-out PSF; (2) the light intensity inside this volume must be thoroughly diminished.

Here, we theoretically and experimentally demonstrate that such a huge three-dimensional light capsule is not a fantasy, but that it can be created using a 3D binary-optical system composed of dielectric grooves in conjunction with a focusing lens, through suppressing the main spot to invert it upside down in PSF and widening the main spot as much as possible – a concept of antiresolution. It is important to note that the 3D distribution of light that is slightly similar to the optical pattern obtained by using the nonhomogenuous medium [14, 15], is rearranged in air without superluminal propagation [16], and exhibits the feature of self-imaging beams in a physical configuration that is distinguished from the classical mathematics-based Guoy effect [17]. It is further shown in our experiment that the focused darkness

with nearly zero-field intensity, embraced by surrounding light, can be $1.69 \times 10^7 \lambda^2$ (with λ being the wavelength of the input light). This unique scheme of light capsule is free of demanding nanofabrication [18], and more importantly, the center position of the darkness can robustly controlled simply by the numerical aperture of the involved focusing lens.

2. Concept and modeling

In optics, the interconnection between the input pattern $O(x, y)$ in the object space and the output pattern $I(x, y)$ in the image space is described with the help of a point spread function (PSF) $P(x, y)$ according to the following relation

$$I(x, y) = \iint\limits_{\text{object plane}} O(\xi, \eta) P(x - \xi, y - \eta) d\xi d\eta. \quad (1)$$

Conventional optical imaging is usually concerned with the PSF's width approaching zero in order to beat the diffraction limit corresponding to Fig. 1b. One interesting question beyond current research focus (engineering Figs. 1b and c) is what new phenomena and applications
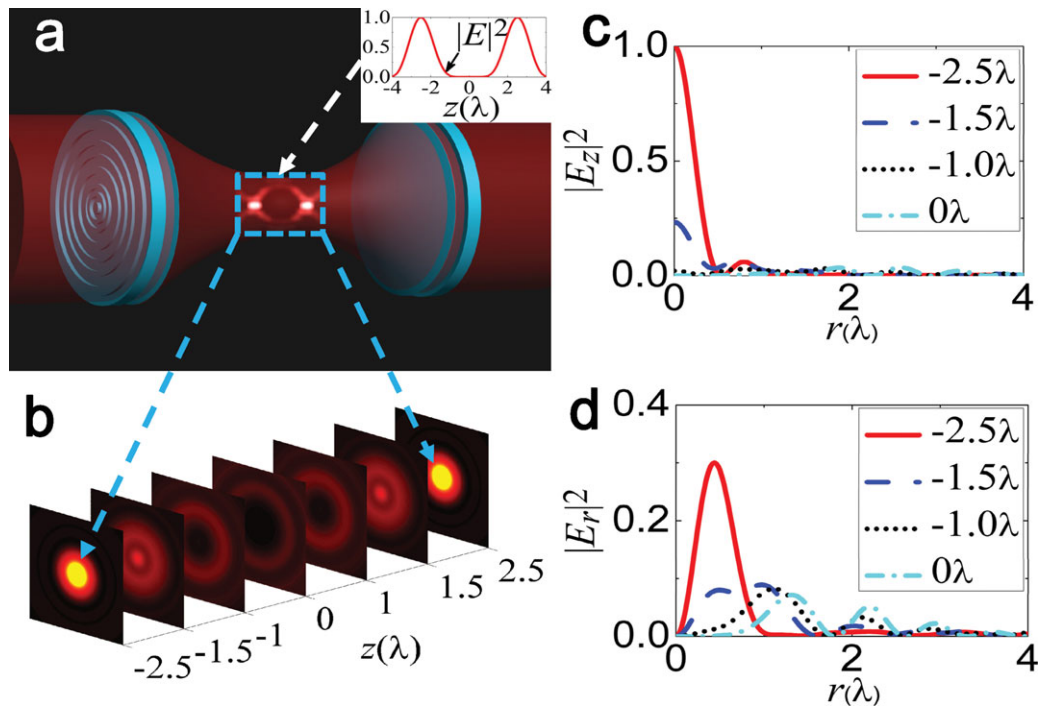
Figure 2 Physical configuration and field distribution of the 3D light capsule. (a) Physical configuration for realizing light capsule, where a Bessel–Gauss beam propagates through a specially designed pairs of binary mask ($r_1 = 0.1163$, $r_2 = 0.5489$, $r_3 = 0.5489$, $r_4 = 0.6022$, $r_5 = 0.7901$, $r_6 = 1$) and focusing lens from the left to right (2 pairs). The inset shows the magnitude of the total electric field along the optical axis, in which a nearly perfect null region (the field amplitude at the order of 10^{-5}) is formed. (b) 7 cut planes of equal separation distances within the dashed box in (a) are selected to demonstrate individual transversal field intensities. (c) Longitudinal polarized field intensity on the first 4 transversal cut planes. (d) Radially polarized field intensity on the first 4 transversal cut planes. The cut plane at $z = 0$ corresponds to the middle plane between the first focus ($z = -2.5 \lambda_0$) and second focus ($z = 2.5 \lambda_0$).

exist if one pushes the limit toward the other extreme, i.e. broadening the PSF as in Fig. 1d, suppressing the main-lobe until it vanishes completely and enhancing the side-lobe as shown in Fig. 1d. The manipulation of PSF for super-resolution in Fig. 1b is completely inverse to that in Fig. 1d. Therefore, we define the concept in Fig. 1d as antiresolution (AR). This scheme can convert "positive" light distribution into "negative" counterpart – darkness. Such a transformation of the PSF for AR can be achieved by putting a 0–π phase lens with a special design of concentric rings, in front of another focusing lens, which works for incident lights of various polarization states, e.g., radially, azimuthally or linearly polarized beams. It is well known that the conventional focusing lens will simply focus the light to its focal point, while Fig. 1e presents the physical scheme for realizing the antiresolution PSF, composed of multibelt dielectric rings and a focusing lens. The dark region in antiresolution PSF is surrounded by the light and spreads smoothly in the focal region, finally forming an optical capsule as shown in Fig. 1f. Although it seems to be the well-known bottle beam generated by interferencing special laser modes [19, 20], our optical capsule-based AR concept contains both bottle beams and hollow-bottle beams [21] as we will show later. More importantly, the theory and procedure of generating optical capsule, which were realized by smearing out PSF macroscopically to achieve AR in supersized volume, have been unanimously developed

and demonstrated. This AR-based scheme, instead of overlapping pre-selected laser modes adopted in conventional methods, incorporate an independent binary lens enabled by a robust design approach semianalytically. Hence, creation of a visible-light capsule can now be accomplished by a diffractive optical device, which no longer needs to manipulate the incident-beam profiles and interferences.

Let us take a Bessel–Gauss beam, the focusing of which we describe via vector diffraction theory [22], as an example. The electric fields near the focus can be obtained for radially polarized light as:

$$E_r = A \int_0^\alpha \sqrt{\cos\theta}\, \sin(2\theta)\ell(\theta)$$
$$\times T(\theta)J_1(kr\sin\theta)e^{ikz\cos\theta}d\theta \qquad (2)$$

$$E_z = 2iA \int_0^\alpha \sqrt{\cos\theta}\, \sin^2\theta\,\ell(\theta)$$
$$\times T(\theta)J_0(kr\sin\theta)e^{ikz\cos\theta}d\theta, \qquad (3)$$
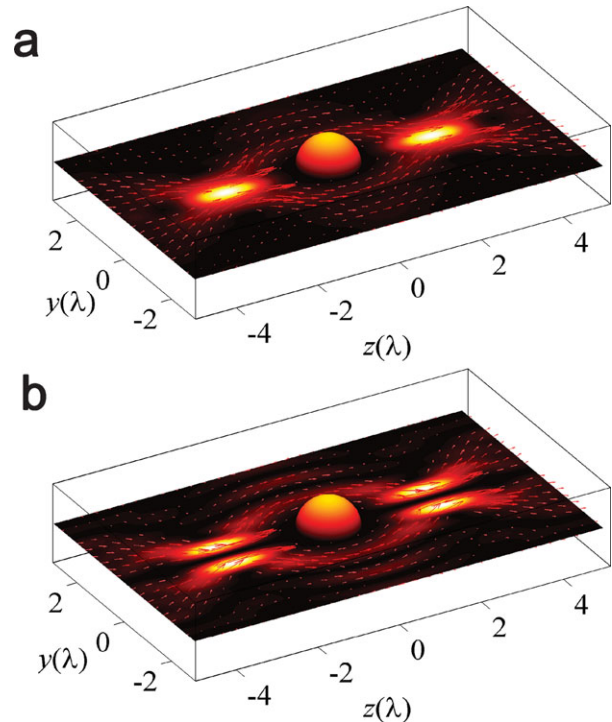
or for azimuthally polarized light:

$$E_\varphi = 2A \int_0^\alpha \sqrt{\cos\theta}\, \sin\theta\,\ell(\theta)T(\theta)J_1(kr\sin\theta)e^{ikz\cos\theta}d\theta, \qquad (4)$$

where $\ell(\theta) = \exp[-\beta^2(\frac{\sin\theta}{\sin\alpha})^2]J_1(2\beta\frac{\sin\theta}{\sin\alpha})$. Here, $k = 2\pi/\lambda$ is the wave vector of light, $\alpha = \arcsin(\mathrm{NA})$, where NA denotes the numerical aperture of the focusing lens. $J_n(x)$ is the nth-order Bessel function of the first kind, and β is the ratio of the pupil radius and the width of the beam waist. A is a constant related to the focal length and the wavelength. $\ell(\theta) = 1$ represents uniform illumination, and $T(\theta) = e^{i\phi(\theta)}$ denotes the transmission function of the binary lens shown in Fig. 1e. A multibelt groove is used as to modulate the phase of the incident light, with $\phi(\theta) = 0$ or $\phi(\theta) = \pi$ at corresponding ranges of angle θ, i.e.

$$T(\theta) = \begin{cases} 1, & \text{for } 0 < \theta < \theta_1, \ \theta_2 < \theta < \theta_3, \ \theta_4 < \theta < \alpha, \\ -1, & \text{for } \theta_1 < \theta < \theta_2, \ \theta_3 < \theta < \theta_4. \end{cases} \quad (5)$$

The angles θ_i correspond to individual radii $r_i = \sin\theta_i/NA$ (normalized by the radius R of the lens). This type of phase modulation was used previously to create longitudinally polarized light [23]. Now we want to calculate a set of θ_i that will produce antiresolution, resulting in the macroscopic perfect darkness where the destructive interference happens by using the 0–π phase modulation of binary lens. We find that the angles θ_i are the physical solution of a nonlinear matrix equation that obeys the gauge of optical vectorial focusing in Eqs. (2)–(4) [24]. We can obtain the angles θ_i for realizing the antiresolution, without any optimization, by solving the nonlinear matrix equation numerically, which is well developed by using Newton theory [25]. It is worthy to point out that one set design of 5-belt binary-phase plate takes only about 2.8 s by solving the nonlinear matrix equation numerically on a 32G-RAM and 8-core-CPU (Intel Core i7) personal computer. The detailed process to solve the nonlinear matrix equation is provided in Supplementary Materials. The field distributions for such a phase mask designed by the mentioned technique are shown in Fig. 2, which has a clear guideline to follow without resorting to blinded optimization. The envelope of the AR region (zero intensity) can be seen from the field cross sections. It is interesting to note that the electric field on the beam axis ($r = 0$) is longitudinally polarized similar to Ref. 23. We can see also that the AR performance of the imaging system is independent of the polarization state of the incident light: it is practically the same for radially and azimuthally polarized light.

Figure 2 presents the physical performance of 3D light capsule with a supersized darkness enclosed. The thickness of concentric dielectric grooves can be designed such that light passing through the groove has an additional π-phase difference compared to that passing through the neighboring air belts [23, 26]. A completely null region in the focal region is formed, i.e. the mainlobe in the PSF vanishes in this region. As a result, the incident probe light has no interaction with the object placed within the null region and just travels around the object. The same lens and complementary SiO_2 grooves can be positioned symmetrically on the other side of the focus point, restoring the incident beam's wavefront. Note that the same system has been validated for a variety of polarizations and wavefronts, e.g., plane waves and Bessel–Gauss beams of different polarization.

Figure 3 Full-wave simulations for energy flux bifurcation and reformation in a light-capsule system at NA = 0.95. (a) Incident light is radial polarized. (b) Incident light is azimuthally polarized. The hollow-bottle beam is generated. A metallic sphere with radius of one wavelength is placed in the center.

Figure 2b presents the field distributions on seven cross-sectional planes at specified locations from the left to the right imaging planes. The envelope of the AR region (the null field) can be seen from the varying sizes of smeared-out regions in Fig. 2b. Note that the electric field on the beam axis ($r = 0$) is purely longitudinally polarized (E_z is the only electric-field component) as Fig. 2c shows. Since such polarization is parallel to the propagation direction, at first glance it seems to violate Maxwell's equations governing the propagation. Nevertheless, when the position is deviating from the beam axis ($r \neq 0$), a radial component E_r starts to emerge as indicated by Fig. 2d, which plays an important role in enabling the energy flux of light to bypass the dark region and reach the second focus. At $z = -2.5\lambda_0$ (i.e. the first imaging plane), E_z clearly dominates within the area close to the beam axis, and therefore the energy of light is prohibited from flowing straightforwardly along the beam axis and has to travel in a curvilinear trajectory. At $z = 0\lambda_0$ (in the middle of two imaging planes), Fig. 2d shows that E_r (corresponding to propagation) is almost smeared out within the central region around the beam axis. When it is more deviated from the center axis, E_r gradually arises, and it corresponds to the propagation and the first color ring in the cut plane at $z = 0\lambda_0$ in Fig. 2b.

Simulations of the Poynting vector $\mathbf{S} = \frac{c}{4\pi}\mathrm{Re}(\mathbf{E} \times \mathbf{H})$ field distribution in Fig. 3 verify the nearly negligible energy in the AR region (~10 orders less than that of the surrounding fields) when an object of the size of one-wavelength
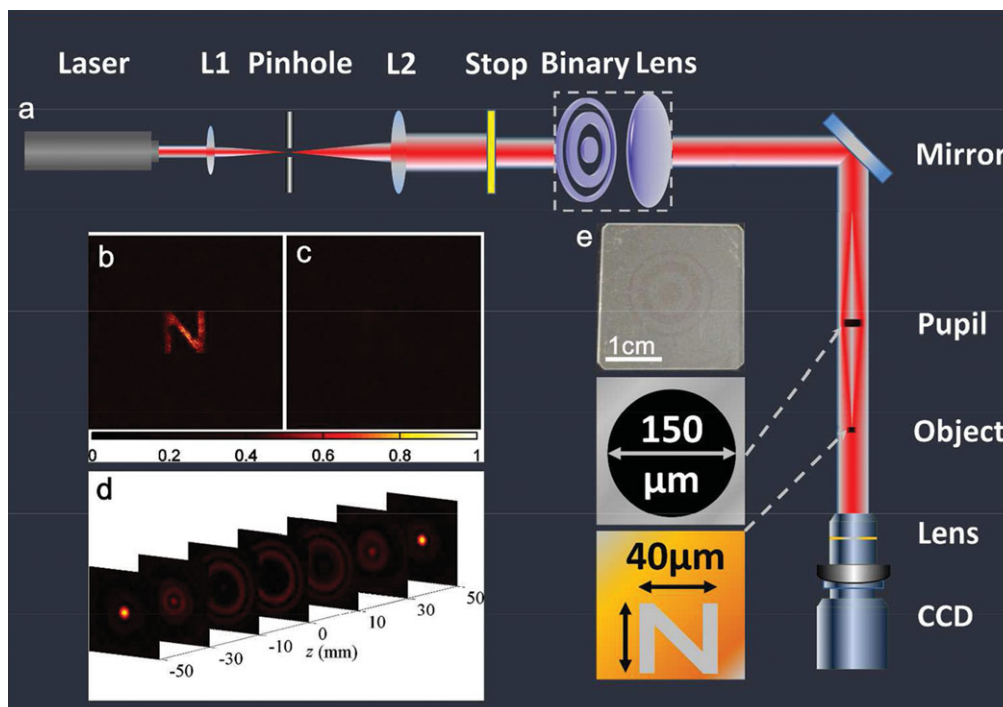
Figure 4 Experimental setup and measurement results for the SAR-based light capsule enclosing supersize darkness region in the imaging system. (a) Schematic of the experiment. Two insets represent the dimension of the opaque pupil and the size of the letter beneath the object, respectively. (b) When the mask phase and the lens phase are simultaneously adopted, light can bypass the opaque pupil and illuminate the object beneath. (c) When either mask or lens phase is adopted separately (i.e. lens or $0-\pi$ modulation mask is removed), the light is blocked by the opaque circular area (150 μm in diameter). Almost no light passes the pupil and a very dark "N" is captured by a CCD. A video (provided as a supplemental multimedia file) shows the switching of the bright and dark "N", corresponding to situations of the presence and absence of $0-\pi$ mask phase. (d) Measured intensity on 7 transversal planes, on both sides of the central plane ($z = 0$). (e) The fabricated binary mask.

radius is placed in the AR region. For exactly the same binary lens and focusing lens as used in Fig. 2a, we consider radially Eq. (2) and azimuthally Eq. (3) polarized incident lights in Figs. 3a and b, respectively. The bifurcation and reformation of energy flux unambiguously reveals that the AR performance is nearly unaffected by the incident polarization states. Hence, any complex polarization state constituted vectorially with radial and azimuthal polarizations can all behave perfectly to yield identical SAR effect. It is also found that the size of AR region (zero-field darkness) can be extremely enlarged by reducing the NA value of the focusing lens ($\sim 1/\text{NA}^3$), while preserving zero intensity in the dark focal field.
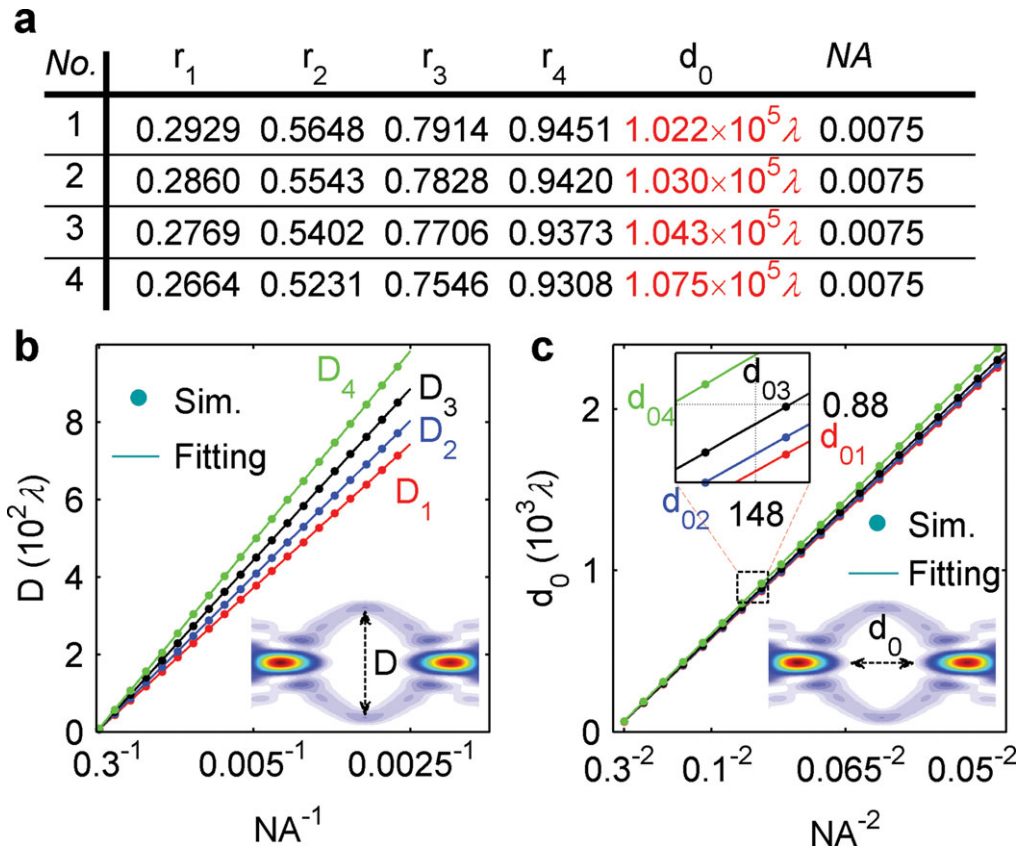
3. Experimental verification

With the experimental setup schematically shown in Fig. 4a, we have experimentally demonstrated an AR-based light capsule embracing significantly large darkness. A pupil made of an opaque gold circular disk (150 μm diameter) is placed at the center of the AR region, which blocks the straight line of sight and serves as an object to be detected. The photograph of fabricated binary mask is shown in Fig. 4e. A gold plate with a letter 'N' etched through is placed behind the pupil to verify the reformation of light

bypassing the pupil. The image of the letter 'N' captured by the CCD camera in Fig. 4b unambiguously evidences that the light can bend and bypass the larger opaque pupil. As a control experiment, when the binary lens is removed, light is fully blocked by the opaque disk of the pupil, resulting in very limited light reaching the letter of the object beneath, and consequently a very dark "N" as shown in Fig. 4c. The envelope of the darkness has been experimentally recorded in Fig. 4d.

With the experimental setup unchanged, a spatial light modulator (SLM) is employed to represent the equivalent phase modulation exerted by the ring belts and lens, as shown in Supplementary Fig. S2a. The phase profile, equivalent to the ring belts and lens, is shown in Fig. S2e. The measurement results are demonstrated in Figs. S2c and S2d, which are in good agreement with the results using actual fabricated binary mask in Fig. 4.

4. Discussion

Figure 5 shows four sets of designed parameters (Fig. 5a) by our optimization-free method and the size (the transversal D in Fig. 5b and axial d_0 in Fig. 5c) dependence of the optical capsule for every case on the NA of the focusing lens. Our theory predicts that the transversal (D) and axial

a

No.	r_1	r_2	r_3	r_4	d_0	NA
1	0.2929	0.5648	0.7914	0.9451	$1.022 \times 10^5 \lambda$	0.0075
2	0.2860	0.5543	0.7828	0.9420	$1.030 \times 10^5 \lambda$	0.0075
3	0.2769	0.5402	0.7706	0.9373	$1.043 \times 10^5 \lambda$	0.0075
4	0.2664	0.5231	0.7546	0.9308	$1.075 \times 10^5 \lambda$	0.0075

Figure 5 The ring belts design and its scaling properties of optical capsule for the lens with different NA. (a) Four sets of parameters that demonstrate the robust design of supersized AR-based light capsule by using the optimization-free method. (b) The radial size (D) of the null field in optical capsule generated by using the lens with different NA (from 0.3 to 0.0025) and the four sets of binary-phase plates in (a). Their fitting curves for different cases are: $D_1 = 1.8600\lambda/NA$ for No. 1 set of ring belt, $D_2 = 2.0117\lambda/NA$ for No. 2, $D_3 = 2.2171\lambda/NA$ for No. 3 and $D_4 = 2.4605\lambda/NA$ for No. 4. For all the four cases, the root-mean-square errors (RMSE) between the original data and fitting curves have the order of magnitude 10^{-14}, indicating a perfect proportion of radial size D to 1/NA. (c) The axial size (d_0) of the null field in optical capsule generated by using the lens with different NA (from 0.3 to 0.05) and four sets of binary-phase plates in (a). Their corresponding fitting curves are: $d_{01} = 5.7728\lambda/NA^2$, $d_{02} = 5.8170\lambda/NA^2$, $d_{03} = 5.8944\lambda/NA^2$ and $d_{04} = 6.0762\lambda/NA^2$ with their fitting RMSEs at the order of magnitude 10^{-12}, implying that the axial size d_0 is proportional to $1/NA^2$.

(d_0) sizes of optical capsule are in proportion to 1/NA and $1/NA^2$, respectively, which is shown in Fig. 5 and Supplementary. Therefore, the size of the optical capsule can be gigantic for low NA. It implies that our design of AR-based 3D light capsule can give rise to a supersized darkness, still surrounded by the light. It unanimously demonstrates the importance of the binary SiO_2 grooves in the creation of nearly perfect darkness enclosed by all light surroundings, which can significantly manipulate the size of darkness embraced by the light while the central location ($z = f_0$) of the darkness and focusing lens' NA in Fig. 1e are unchanged. In Figs. 5b and c, the fact that one binary-phase plate works very well for all the focusing lenses with different NA in generating the optical capsule, unveils the intrinsic property of the well-designed binary-phase plate: it can still generate the optical capsule with the huge-size darkness at its far-field (Fraunhofer) diffraction region even if the focusing lens does not exist in Fig. 1e. In fact, the role that the focusing lens in Fig. 1e has played is just pulling the far-field diffraction region of the binary-phase plate to the region near the focal plane of the focusing lens, which has been confirmed in Fourier optics [1]. As a result, the size of the optical capsule near the focal region is tightly dependent on the lens's functionality: the weak (low-NA) focusing lens leads to an optical capsule with large-size darkness, while the strong (high-NA) focusing lens results in an optical capsule with small-size darkness, which is proved by Figs. 5b and c. Therefore, in physics, the most primitive root for the generation of optical capsule presented in the scheme of Fig. 1e is the binary-phase plate's substantial ability in forming the gigantic darkness (impossible to be detected directly without the focusing lens) surrounded by light at the far-field diffraction region.

5. Conclusion

In summary, an optical scheme for realizing a supersized light capsule by creating an antiresolution region with a binary phase ($0-\pi$) mask was presented theoretically and

experimentally in air. The scheme is also adjustable, namely, the volume of darkness inside the light capsule can be changed in a drastically wide range, while the binary phase mask can be kept unchanged (only depending on NA of the focusing lens). We stress that the "bending of light" is in dramatic contrast to the Airy beam that is actively studied in plasmonics [27, 28]. Our proposal of "light bending" is immune to energy loss, narrow operation bandwidth, limited SAR area, superluminal propagation, or polarization sensitivity. This new scheme of maneuvering light creates a plethora of possibilities for optical imaging systems, superb surveillance by seeing things behind objects for military use.

References

[1] M. Born and E. Wolf, Principles of Optics (Cambridge University Press, Cambridge, 1999).

[2] C. S. Williams, and O. A. Becklund, Introduction to the Optical Transfer Function (Wiley, New York, 1989).

[3] E. Wolf, Proc. R. Soc. Lond. A **253**, 349 (1959); E. Wolf, Proc. R. Soc. Lond. A **253**, 358 (1959).

[4] J. B. Pendry, Phys. Rev. Lett. **85**, 3966 (2000).

[5] N. Fang, H. Lee, C. Sun, and X. Zhang, Science **308**, 534 (2005).

[6] T. Taubner, D. Korobkin, Y. Urzhumov, G. Shvets, and R. Hillenbrand, Science **313**, 1595 (2006).

[7] I. I. Smolyaninov, Y. J. Huang, and C. C. Davis, Science **315**, 1699 (2007).

[8] X. Zhang and Z. Liu, Nature Mater. **7**, 435 (2008).

[9] Z. W. Liu, et. al., Science **315**, 1686 (2007); D. Lu and Z. W. Liu, Nature Commun. **3**, 1205 (2012).

[10] F. M. Huang and N. I. Zheludev, Nano Lett. **9**, 1249 (2009); E. T. F. Rogers, et. al., Nature Mater. **11**, 432 (2012).

[11] J. Rho, et. al., Nature Commun. **1**, 143 (2010).

[12] K. I. Willig, S. O. Rizzoli, V. Westphal, R. Jahn, S. W. Hell, Nature **440**, 935 (2006); E. Rittweger, K. Y. Han, S. E. Irvine, C. Eggeling, and S. W. Hell, Nature Photon. **3**, 144 (2009).

[13] S. Van de Linde, A. Loschberger, T. Klein, M. Heidbreder, S. Wolter, M. Heilemann, and M. Sauer, Nature Photon. **6**, 991 (2011); B. Huang, W. Wang, M. Bates, and X. Zhuang, Science **319**, 810 (2012).

[14] J. B. Pendry, D. Schurig, and D. R. Smith, Science **312**, 1780 (2006).

[15] U. Leonhardt, Science **312**, 1777 (2006).

[16] J. Perczel, T. Tyc, and U. Leonhardt, New J. Phys. **13**, 083007 (2011).

[17] J. Courtial, Optics Commun. **151**, 1–4 (1998).

[18] J. Valentine, J. Li, T. Zentgraf, G. Bartal, X. Zhang, Nat. Mater. **8**, 568 (2009); T. Ergin, N. Stenger, P. Brenner, J. B. Pendry, and M. Wegener, Science **328**, 337 (2010).

[19] J. Arlt and M. J. Padgett, Opt. Lett. **25**, 191 (2000).

[20] I. Chremmos, P. Zhang, J. Prakash, N. K. Efremidis, D. N. Christodoulides, and Z. Chen, Opt. Lett. **36**, 3675 (2011).

[21] H. P. Ye, C. Wan, K. Huang, T. C. Han, J. H. Teng, Y. S. Ping, and C. W. Qiu, Opt. Lett. **39**, 630 (2014).

[22] K. S. Youngworth and T. G. Brown, Opt. Exp. **7**, 77 (2000); H. Ye, C.-W. Qiu, K. Huang, J. Teng, B. Luk'yanchuk, and S. P. Yeo, Laser Phys. Lett. **10**, 065004 (2013).

[23] H. Wang, L. Shi, B. Lukyanchuk, C. Sheppard, C. T. Chong, Nature Photon. **2**, 501 (2008); K. Huang, S. Peng, X. Kang, X. Zhang, and Y. Li, Opt. Lett. **35**, 965 (2010).

[24] K. Huang, H. P. Ye, J. H. Teng, S. P. Yeo, B. Luk'yanchuk, and C. W. Qiu, Laser Photon. Rev. **8**, 152 (2014).

[25] J. E. Dennis and R. B. Schnabel, Numerical Methods for Unconstrained Optimization and Nonlinear Equations (Prentice-Hall, New Jersey, 1983).

[26] C. J. R. Sheppard and T. Wilson, Opt. Acoust. **2**, 105 (1978); Q. Zhan, W. Chen, and J. Wang, SPIE Newsroom, DOI: 10.1117/2.1201103.003522, 2011.

[27] A. Minovich, et. al., Phys. Rev. Lett. **107**, 116802 (2011).

[28] P. Zhang, et. al., Opt. Lett. **36**, 3191 (2011).